

Controls on the barium isotope compositions of marine sediments

Luke Bridgestock^{a*}, Yu-Te Hsieh^a, Donald Porcelli^a, William B. Homoky^a, Allison
Bryan^a, Gideon M. Henderson^a

^a Department of Earth Sciences, University of Oxford, South Parks Road, Oxford,
OX1 3AN, UK

*Corresponding author; luke.bridgestock@earth.ox.ac.uk

Keywords: Barium isotopes; marine sediments; marine barium cycle; paleo-
oceanography; GEOTRACES

Highlights:

1. Detrital and authigenic Ba in marine sediments have distinct isotope compositions
2. Sinking particles predicted to have similar isotope compositions to authigenic Ba
3. Ba removal to sediments has an isotope fractionation of $\Delta^{138/134}\text{Ba} \approx +0.4$ to $+0.5$
4. Sedimentary Ba isotope compositions record perturbations to upper ocean Ba cycling

Abstract; 254 words

Main text; 5,885 words

Abstract

The accumulation of barium (Ba) in marine sediments is considered to be a robust proxy for export production, although this application can be limited by uncertainty in BaSO₄ preservation and sediment mass accumulation rates. The Ba isotope compositions of marine sediments could potentially record insights into past changes in the marine Ba cycle, which should be insensitive to these limitations, enabling more robust interpretation of sedimentary Ba as a proxy. To investigate the controls on the Ba isotope compositions of marine sediments and their potential for paleo-oceanographic applications, we present the first Ba isotope compositions results for sediments, as well as overlying seawater depth profiles collected in the South Atlantic. Variations in Ba isotope compositions of the sediments predominantly reflect changes in the relative contributions of detrital and authigenic Ba sources, with open-ocean sediments constraining the isotope composition of authigenic Ba to be $\delta^{138/134}\text{Ba} \approx +0.1 \text{ ‰}$. This value is consistent with the average isotope composition inferred for sinking particulate Ba using simple mass balance models of Ba in the overlying water column and is hypothesized to reflect the removal of Ba from the upper water column with an associated isotopic fractionation of $\Delta^{138/134}\text{Ba}_{\text{diss-part}} \approx +0.4$ to $+0.5$. Perturbations to upper ocean Ba cycling, due to changes in export production and the supply of Ba via upwelling, should therefore be recorded by the isotope compositions of sedimentary authigenic Ba. Such insights will help to improve the reliable application of Ba accumulation rates in marine sediments as a proxy for past changes in export production.

1. Introduction

Interest in the marine biogeochemical cycle of barium (Ba) has been largely motivated by its potential to trace aspects of the marine organic carbon cycle. In particular, the accumulation of Ba in marine sediments is considered to be a robust proxy for export production in the modern (e.g. Eagle et al., 2003) and past oceans (e.g. Paytan & Griffiths, 2007). Inventories of suspended particulate Ba have also been used to study the remineralization of exported organic carbon in mesopelagic waters (e.g. Cardinal et al., 2005, Jacquet et al., 2015). The precipitation of barite (BaSO_4) is the dominant oceanic sink of Ba, and forms the basis of these proxy applications (Dehairs et al., 1980). The vast majority of the global ocean is undersaturated with respect to this mineral, therefore BaSO_4 precipitation is thought to occur in supersaturated micro-environments during the bacterial decay of organic aggregates, and/or through the dissolution of acantharian celestite (SrSO_4) skeletons (Monnin et al., 1999, Bishop, 1988, Ganeshram et al., 2003, Bernstein & Byrne, 2004). The precipitation of BaSO_4 is considered to predominantly occur within mesopelagic waters, where the majority of organic carbon remineralization takes place, although it can potentially occur at any depth throughout the water column (Dehairs et al., 1980, Dymond et al., 1992, Legeleux & Reyss, 1996, Cardinal et al., 2005, van Beek et al., 2007, 2009).

The use of sedimentary Ba accumulation rates as a proxy for export production is founded on the observation that fluxes of particulate Ba sinking through the water column are typically correlated with those of particulate organic carbon, although there is significant variability in the ratio of these two components both spatially and temporally (Dymond et al., 1992, Francois et al., 1995, Dymond &

Collier, 1996, Dehairs et al., 2000, McManus et al., 2002, Balakrishnan Nair et al., 2005, Sternberg et al., 2007). Once buried below the sediment-water interface, BaSO₄ particles appear to be well preserved (Paytan & Kastner, 1996), provided that pore waters are not depleted in SO₄²⁻ (e.g. Torres et al., 1996). High preservation rates of BaSO₄, at least in oxic sediments, compared to biogenic sedimentary components such as organic carbon, CaCO₃ and opal, make Ba accumulation rates a robust proxy for export production (e.g. Dymond et al., 1992).

Preservation rates of BaSO₄ at the sediment-water interface however are known to be variable in the modern ocean (Fagel et al., 2002). This is a source of uncertainty for reconstructions of export production in the past, which could be exacerbated by changes in the saturation state of the ocean with respect to BaSO₄ through time (e.g. Dickens et al., 2003). The concentration of Ba in marine sediments is also significantly affected by dilution due to the accumulation of other sedimentary components (e.g. CaCO₃), requiring conversion to Ba accumulation rates using age models or constant flux proxies such as ²³⁰Th or extraterrestrial ³He (Paytan & Griffith, 2007). Uncertainty in establishing bulk sediment accumulation rates can produce significant uncertainty in Ba accumulation rates, which can affect the apparent timing and magnitude of inferred changes in export production (Anderson & Winckler, 2005, Torfstein et al., 2010). Detrital inputs of aluminosilicate minerals can also compromise export production estimates derived from Ba accumulation rates, particularly in settings close to the continental margin (Dymond et al., 1992, Reitz et al., 2004),

Improved understanding of the ocean and sedimentary cycling of Ba would be beneficial for reliable application of the Ba proxy for export production. Recent studies have shown that the removal of Ba from the upper ocean is associated with an

isotopic fractionation with a preference for the lighter isotopes (Horner et al., 2015, Bates et al., 2017, Hsieh & Henderson, 2017). Barium isotope composition variations therefore have the potential to offer insights into the different sources and sinks of Ba in the water column. The Ba isotope compositions of marine sediments may record insights into changes in the marine Ba cycle in the past, which should be insensitive to variable BaSO₄ preservation and dilution by biogenic sedimentary components, enabling more robust interpretations of the Ba proxy for export production. However, the magnitude of the isotope fractionation accompanying Ba removal from the ocean is currently poorly constrained, as are the controls on the Ba isotope compositions of marine sediments. To address these issues and to investigate the potential of Ba isotope compositions of marine sediments for paleo-oceanographic reconstructions, we present the first Ba isotope composition data for marine sediments, in addition to overlying seawater depth profiles from the South Atlantic.

2. Samples and hydrography

Seawater and sediment samples analyzed in this study were collected during the JC068 expedition (December, 2011 – January, 2012) as part of the GEOTRACES GA10 section, on board the RSS James Cook (Fig. 1).

A total of 49 seawater samples were measured for Ba concentrations and isotope compositions in this study, taken from four water-column profiles, extending from the continental slope of the Uruguayan margin (stations 21 and 22), to the Argentine Basin (station 18) and mid Atlantic Ridge (station 12). In addition Ba concentration and isotope composition results for a seawater depth profile collected at station 20 previously published by Hsieh & Henderson (2017) are included. Six

sediment cores were collected from the continental shelf and slope of the Uruguayan margin, the abyssal plain of the Argentine Basin and the mid Atlantic Ridge (Fig. 1). A total of 93 sediment samples from these cores were measured for Ba and Al concentrations, with 58 of these samples analyzed for Ba isotope compositions.

The water masses encountered on the GEOTRACES GA10 section are distinguished by their distinct salinity values (Fig. 1b). Hydrographic data for this cruise transect are available as part of the GEOTRACES data product (Mawji et al., 2015).

Seawater was collected using either a stainless steel or titanium rosette each equipped with 24 Ocean Test Equipment sampling bottles. Seawater was filtered on-board into acid-cleaned polypropylene bottles using 0.45 μm Acropak capsule filters, before being acidified to $\text{pH} \approx 1$ to 2 by addition of distilled HCl. Sediment cores were collected using a Bowers and Connelly Megacore, retrieving between 10 and 36 cm of the surface sediments with intact sediment-water interfaces (Homoky et al., 2013). Following extraction of the pore waters, the residual sediment was divided at 1 to 2 cm depth intervals using a Teflon sheet. Sediments from the individual depth intervals were subsequently freeze-dried and homogenized by agate pestle and mortar. Pore water data for NO_3^- and Fe indicate that pore waters over the sampled depth ranges of the sediment cores are not likely to be depleted in SO_4^{2-} (Supplementary Material).

3. Analytical techniques

Sample preparation and analyses were conducted at the University of Oxford. The Ba isotope compositions of seawater and sediment samples were determined

using thermal ionization mass spectrometry (TIMS), with the application of a ^{137}Ba – ^{135}Ba double spike to correct for instrumental mass bias (Hsieh & Henderson, 2017). Approximately 50 ml of seawater was accurately weighed and equilibrated with a known quantity of Ba double spike solution. The Ba was then co-precipitated with CaCO_3 by addition of 3 ml of a 0.9 M Na_2CO_3 solution, prior to purification by cation exchange chromatography (Supplementary Material; Foster et al., 2004, Nan et al., 2015, Horner et al., 2015). Organics leached from the cation exchange resin were oxidized by the sequential addition and evaporation of 7.5M HNO_3 and 9.8M H_2O_2 . The procedural blank was typically < 1 ng ($n = 5$); however on two occasions it was slightly higher at 3 and 4 ng of Ba. These values, typically representing < 0.4 %, and in the worst case < 1.6 % of the Ba processed in the samples (≈ 250 to 700 ng), are considered to have a negligible impact on the quality of the data, and hence no blank corrections were applied.

For the sediment samples, between 0.3 to 0.9 g of powdered sediment was accurately weighed into Teflon vials, prior to total digestion in 1.25 ml 16M HNO_3 + 3.75 ml 12M HCl at 60°C , followed by 3 ml 28M HF + 2.25 ml 11.6M HClO_4 at 150°C and finally 2 ml 11.6M HClO_4 at 150°C to 180°C , after Homoky et al. (2011). Residual HClO_4 was removed by the repeated addition and evaporation of 1 – 2 ml 16M HNO_3 at 150°C to 200°C . The digested samples were then re-dissolved in 10 ml 0.5M HNO_3 . The Ba and Al contents of the digested solutions were determined using magnetic sector inductively coupled plasma mass spectrometry (ICP-MS; Thermo Scientific, Element 2), with the addition of Rh as an internal standard.

Aliquots of the digested solutions, containing about 1000 ng Ba, were taken for determination of Ba isotope compositions. Appropriate quantities of the ^{137}Ba – ^{135}Ba double spike solution were equilibrated with the sample aliquots prior to

purification of Ba by cation exchange chromatography (Supplementary Material; Foster et al., 2004, Hsieh & Henderson, 2017). Organics leached from the cation exchange resin were subsequently oxidized by the sequential addition and evaporation of 7.5M HNO₃ and 9.8M H₂O₂. The procedural blank was consistently determined to be < 1.6 ng (n = 9), representing < 0.16 %, of the Ba processed in the samples, hence no blank corrections were applied.

The purified Ba was loaded onto previously outgassed single Re filaments, along with 1 µl of a Ta₂O₅ – H₃PO₄ activator gel as described by Hsieh & Henderson (2017). More stable ion beams were achieved by loading the activator gel onto the filament before the sample. The Ba isotope measurements were conducted using a Thermo Scientific TRITON TIMS instrument. Filaments were heated to between 1500°C and 1550°C within about 30 to 40 mins. Higher and more stable ion beams were typically achieved if filaments were initially heated to approximately 1600°C, before cooling to between 1500°C and 1550°C. The resulting ion beam intensities were typically 5 to 8 V for the most abundant isotope, ¹³⁸Ba. During each analysis, ion beams at atomic masses 134 (Ba), 135 (Ba), 136 (Ba), 137 (Ba), 138 (Ba), 139 (La) and 140 (Ce) were monitored simultaneously using Faraday cups equipped with 10¹¹ Ω resistors. Following a peak center, ion beams were collected in 54 blocks of 10 integrations lasting 8.4 seconds each. Between each block, ion beams were deflected to measure the electronic baseline. The ion beams at atomic masses 139 (La) and 140 (Ce) were monitored to assess potential isobaric inferences on ¹³⁶Ba and ¹³⁸Ba, and during all analyses displayed no detectable signal.

The raw isotopic ratios were processed offline to correct for instrumental mass bias (Hsieh & Henderson, 2017). The Ba isotope compositions are expressed as

$\delta^{138/134}\text{Ba}$ values, which are parts per thousand deviations from a Ba standard reference material (SRM) NIST 3104a (eqn. 1).

$$\delta^{138/134}\text{Ba} = \left(\frac{{}^{138}\text{Ba}}{{}^{134}\text{Ba}}_{\text{sample}} / \frac{{}^{138}\text{Ba}}{{}^{134}\text{Ba}}_{\text{NIST3104a}} - 1 \right) \times 1000 \quad (1)$$

The isotopic results were also used to obtain Ba concentrations of seawater samples by isotope dilution.

4. Results

Repeat analyses of SRM NIST3104a, at similar ion beam intensities to those of sample measurements result in external reproducibility of $\delta^{138/134}\text{Ba}$ of ± 0.03 , or better (2SD; see Supplementary Material). This level of uncertainty is taken to represent that of the samples, and is justified by the agreement displayed by duplicate measurements of certain seawater (Fig. 2; Fig. 3; Supplementary Data 1) and sediment samples (Fig. 4; Supplementary Data 2). Further validation is provided by 7 repeat analyses of two different seawater samples collected in the North Atlantic, which yield external reproducibility for $\delta^{138/134}\text{Ba}$ of ± 0.003 and ± 0.01 (2SD; Hsieh & Henderson, 2017). The Ba concentrations of these replicate seawater analyses display a reproducibility of ± 2 to 3% (RSD) which is taken to represent the uncertainty of the seawater Ba concentrations.

4.1 Dissolved Ba concentrations and isotope compositions of seawater samples

From the surface to the deep ocean, dissolved Ba concentrations increase from approximately 40 to 100 nmol kg⁻¹, while $\delta^{138/134}\text{Ba}$ values decrease from approximately +0.6 to +0.2 ‰ (Fig. 2; Supplementary Data 1). Consequently, Ba concentrations and $\delta^{138/134}\text{Ba}$ values display a strong negative correlation ($r^2 = 0.89$), with the exception of one anomalous sample from station 20, previously published by Hsieh & Henderson (2017) (Fig. 3).

In general, Ba concentrations and $\delta^{138/134}\text{Ba}$ values are relatively constant in the upper 200 to 400 m of the water column (Fig. 2), consistent with previous observations elsewhere in the ocean (Horner et al., 2015, Bates et al., 2017, Hsieh & Henderson, 2017). Laterally along the sampled transect, upper water column (200 m) dissolved Ba concentrations and $\delta^{138/134}\text{Ba}$ values are also uniform at 43.3 ± 4.2 nmol kg⁻¹ and $+0.57 \pm 0.04$ ‰ (2SD; $n = 17$). Between about 200 to 1000 m water depth, Ba concentrations and $\delta^{138/134}\text{Ba}$ values increase and decrease respectively, to 70 to 80 nmol kg⁻¹ and +0.35 to +0.40 ‰ (Fig. 2). Barium concentrations and isotope compositions then remain relatively constant until about 3000 m water depth where Antarctic Bottom Water is encountered, with Ba concentrations increasing to between 90 to 110 nmol kg⁻¹, and $\delta^{138/134}\text{Ba}$ values decreasing to about +0.25 ‰. At station 21, a minimum in Ba concentrations (and maximum in $\delta^{138/134}\text{Ba}$ values) is observed at 2500 m water depth. Notably a minimum is also observed at this location and depth for the concentrations of the macro-nutrients nitrate, phosphate and silicate, in addition to the micro-nutrient Zn, which presumably represents a hydrographic feature (Wyatt et al., 2014).

The general distribution of Ba concentrations and $\delta^{138/134}\text{Ba}$ values, in addition to their co-variance, are consistent with previous results from the North Atlantic, South Atlantic, Southern Ocean and North Pacific (Horner et al. 2015, Bates et al.,

2017, Hsieh & Henderson, 2017; Fig. 3). In particular, results for station 12 are in good agreement with the results published by Horner et al. (2015) and Bates et al. (2017) determined at stations 3 and 6 from the GEOTRACES GA10 section (Supplementary Material; Fig.1). Notably, these datasets were produced at a different laboratory, using different analytical techniques (i.e. using multiple collector ICP-MS) than the data presented in this study.

4.2 Elemental concentrations and Ba isotope compositions of sediment samples

The underlying sediments exhibit lower $\delta^{138/134}\text{Ba}$ values than the seawater samples, ranging between -0.09 to +0.10 ‰ (Fig. 4, Supplementary Data 2). The Ba concentrations of the sediments range from 371 to 1104 $\mu\text{g g}^{-1}$, while Ba/Al mass ratios range between 0.005 and 0.053. In detail, the cores collected on the continental shelf and slope (stations 21, 22, 23 and 24) exhibit relatively low Ba/Al ratios of 0.005 to 0.009, while the cores collected on the abyssal plain of the Argentine Basin and the mid Atlantic ridge generally exhibit higher Ba/Al ratios of 0.006 to 0.05 (Fig. 4). The $\delta^{138/134}\text{Ba}$ values generally increase with increasing Ba/Al ratio (Fig. 5).

5. Discussion

5.1 The isotope compositions of sedimentary Ba sources

Inputs of detrital aluminosilicate minerals can provide significant contributions to marine sedimentary Ba inventories, particularly at locations close to the continental margin (e.g. Klump et al., 2000). To assess the importance of detrital

Ba inputs to marine sediment, Ba/Al ratios have commonly been applied in previous studies (e.g. Klump et al., 2000, Pfeifer et al., 2001, Reitz et al., 2004). In this study, the lower Ba/Al ratios determined for sediments collected on the continental shelf and slope, compared to those collected on the abyssal plain and mid Atlantic Ridge, reflects higher contributions of detrital Ba to the former sites (Fig. 4). By assuming a Ba/Al ratio for the detrital component of the sediment, it is possible to estimate the fractional contributions of Ba from detrital and non-detrital sources (eqn. 2).

$$Ba_{\text{excess}} (\%) = (1 - [(Ba/Al_{\text{detrital}} \times Al_{\text{total}})/Ba_{\text{total}}]) \times 100 \quad (2)$$

Where Ba_{excess} denotes Ba from non-detrital sources, Ba_{total} and Al_{total} denote the total Ba and Al concentrations of the sediment, and Ba/Al_{detrital} denotes the reference ratio of the detrital material. The accuracy of sedimentary Ba_{excess} contribution assessment using this approach primarily depends on the appropriate choice of Ba/Al_{detrital} reference ratio, which is known to display regional variations (Klump et al., 2000, Reitz et al., 2004). The lowest Ba/Al ratios for our sediment samples are observed at station 23, with a single sample featuring a Ba/Al ratio of 0.005 and the remainder of about 0.006 (Fig. 4, Fig. 5, Supplementary Data 2). These values provide an upper limit for the appropriate Ba/Al_{detrital} for assessment of Ba_{excess} values, and are in good agreement with Ba/Al_{detrital} ratios suggested by Pfeifer et al. (2001) for sediments from this region, of 0.0048 to 0.006. Using $Ba/Al_{\text{detrital}} = 0.0055 \pm 0.0005$, the estimated proportions of Ba_{excess} range between 0 and 90% (Fig. 4c, Fig. 5, Supplementary Data 2).

There is a positive correlation between $\delta^{138/134}\text{Ba}$ values and Ba_{excess} , which represents a mixing line between detrital and excess Ba, each featuring a distinct

isotope composition (Fig. 5). Through extrapolation, it can be inferred that excess Ba exhibits slightly higher $\delta^{138/134}\text{Ba}$ values ($\approx +0.1\text{‰}$) than detrital Ba ($\delta^{138/134}\text{Ba} \approx -0.1$ to 0‰). The observed sediment $\delta^{138/134}\text{Ba}$ values do display subtle deviations from this linear correlation that exceed analytical uncertainty. Without better constraints however, it is not possible to ascertain whether these subtle variations are caused by small variations in the isotope composition of excess Ba, or of detrital Ba or $\text{Ba}/\text{Al}_{\text{detrital}}$ for individual samples. For example, sediments from station 18 exhibit down core variations in $\text{Ba}_{\text{excess}}$ of approximately 60% to 10%, but display reasonable constant $\delta^{138/134}\text{Ba}$ values of $+0.01 \pm 0.03\text{‰}$ (mean $\pm 2\text{SD}$; $n = 19$) (Fig. 4; Fig. 5; Supplementary Data 2). This could indicate that both detrital and excess Ba have similar $\delta^{138/134}\text{Ba}$ values at this site (of $\approx +0.01\text{‰}$), or that there are subtle down-core variations in $\delta^{138/134}\text{Ba}$ values of one or both of these endmembers, coinciding with the change in $\text{Ba}_{\text{excess}}$.

Difficulty in precisely calculating $\delta^{138/134}\text{Ba}$ values of excess Ba throughout the sample set described above unfortunately precludes more detailed assessment of the factors that could potentially cause subtle variations in the isotope composition of excess Ba, both spatially across the sampled transect and within individual cores. For example, isotopic variability in excess Ba due to diagenetic processes, or factors such as water depth and barite saturation state of bottom waters, cannot be ruled out but cannot be clearly resolved. In any case the total range of sediment Ba isotope compositions are limited to 0.2‰ , and the dominant control on the observed isotopic variations is the proportion of $\text{Ba}_{\text{excess}}$ (Fig. 5). Therefore any potential variations in the Ba isotope compositions of excess Ba in the sample set are likely to be less than 0.1‰ . This discussion illustrates the challenge of accurately and precisely correcting Ba excess $\delta^{138/134}\text{Ba}$ values for detrital Ba inputs. Studies attempting to discern subtle

isotopic variations in excess Ba will therefore need to carefully choose their sampling sites to feature sediments with low detrital Ba contributions, which are typically found in settings away from continental margins.

The inferred isotope composition of excess Ba is primarily constrained by results for sediments from station 8, which feature particularly low detrital Ba contributions (Fig. 5), and are characterized by $\delta^{138/134}\text{Ba} = +0.09 \pm 0.01 \text{ ‰}$ (mean \pm 2SE, $n = 10$). It is likely that BaSO_4 is the dominant phase hosting the excess Ba in these sediments, but other phases such as carbonate minerals, organic matter or Fe-Mn phases could also potentially be important (e.g. Eagle et al., 2003). Sediments from station 8 are composed of 70 to 83 wt.% carbonate and 0 to 0.3 wt.% total organic carbon (Supplementary Material; Supplementary Data 2). Following the approach of Gingele & Dahmke (1994), and assuming this carbonate and organic carbon have Ba concentrations of $30 \mu\text{g g}^{-1}$ and $60 \mu\text{g g}^{-1}$ respectively, we estimate that these phases only contribute up to 5.7 % and 0.03 % of the excess Ba in these sediments. This analysis supports the interpretation that the $\delta^{138/134}\text{Ba}$ values inferred for excess Ba, of $+0.09 \pm 0.01 \text{ ‰}$, predominantly represents that of BaSO_4 , although minor Ba contributions from Fe-Mn phases may also be possible. Regardless, the $\delta^{138/134}\text{Ba}$ values of sediments from station 8 provide an important first constraint on the isotope composition of Ba exported to the sediment through biogeochemical processes occurring in the overlying water column.

5.2 The Ba isotope systematics of seawater

To understand the Ba isotope composition of sediments, particularly the authigenic Ba, requires assessment of the controls on Ba isotope composition imparted by processes in the overlying water column.

Depth profiles of Ba concentrations display quasi-nutrient type distributions reflecting the net removal of Ba in the upper ocean, and a net regeneration at depth (e.g. Jeandel et al., 1996; Fig. 2). Unlike true nutrient elements, however, Ba is not quantitatively removed or regenerated during its vertical cycling, and is not known to be actively taken up by marine phytoplankton (Paytan & Griffiths, 2007). The precipitation of BaSO₄ in supersaturated micro-environments, coupled with the subsequent dissolution of BaSO₄ particles in the under-saturated water column and at the sediment-water interface, are thought to be the dominant processes controlling the water-column distribution (e.g. Jeandel et al., 1996, Hoppema et al., 2010, Jacquet et al., 2016). Passive removal by organic material and biogenic CaCO₃, as well as by scavenging by Fe-Mn phases, may also influence the cycling of Ba in the ocean, although the distribution and importance of such processes is poorly understood (Dehairs et al., 1980, Dymond et al., 1992, Balakrishnan Nair et al., 2005, Sternberg et al., 2005). Ocean circulation acts to redistribute and mix these signals, hence the distribution of dissolved Ba in the ocean represents a combination of removal and regeneration processes, interacting with water mixing and advection (e.g. Horner et al., 2015, Bates et al., 2017, Hsieh & Henderson, 2017).

With the exception of the data presented by Cao et al. (2016) from the East and South China Seas, previous studies found a strong co-variance between dissolved Ba concentrations and isotope compositions at sites throughout the global ocean (Horner et al., 2015, Bates et al. 2017, Hsieh & Henderson, 2017; Fig. 3). The results obtained here are in good agreement with this relationship. Such a tight coupling

between dissolved Ba concentrations and $\delta^{138/134}\text{Ba}$ values requires that removal, regeneration and mixing processes all act to produce similar relationships between these parameters.

We apply simple models to consider the effects of Ba removal and regeneration processes, and water mass mixing on the observed Ba concentration- $\delta^{138/134}\text{Ba}$ systematics. Steady state fractionation models have previously been used to describe the partitioning of Ba between dissolved and particulate phases in the ocean with an associated isotope fractionation (Horner et al., 2015, Bates et al., 2017, Hsieh & Henderson, 2017), and the following equation has been widely used:

$$\delta^{138/134}\text{Ba}_{\text{diss}} = \delta^{138/134}\text{Ba}_{\text{diss}, 0} + [1000 \times (\alpha_{\text{diss/part}} - 1)] \times (1 - f_{\text{diss}}) \quad (3)$$

where f_{diss} denotes the fraction of dissolved Ba remaining in seawater relative to the initial concentration, and $\delta^{138/134}\text{Ba}_{\text{diss}}$ and $\delta^{138/134}\text{Ba}_{\text{diss}, 0}$ denote current and the initial isotope composition of dissolved Ba, respectively. The isotope fractionation factor, $\alpha_{\text{diss/part}}$, is defined as the $^{138}\text{Ba}/^{134}\text{Ba}$ ratio of dissolved Ba ($_{\text{diss}}$), relative to the $^{138}\text{Ba}/^{134}\text{Ba}$ ratio of particulate Ba ($_{\text{part}}$).

The effect of Ba addition to deep waters by regeneration processes on dissolved Ba concentrations and $\delta^{138/134}\text{Ba}$ values in the water column can be calculated through isotopic mass balance (eqn. 4).

$$\delta^{138/134}\text{Ba}_{\text{diss}} = (\delta^{138/134}\text{Ba}_{\text{pre}} \times f_{\text{pre}}) + (\delta^{138/134}\text{Ba}_{\text{regen}} \times f_{\text{regen}}) \quad (4)$$

Where $\delta^{138/134}\text{Ba}_{\text{pre}}$ and $\delta^{138/134}\text{Ba}_{\text{regen}}$ denote the isotope compositions of the ‘preformed’ Ba in the water, and the regenerated flux respectively, with f_{pre} and f_{regen}

representing the fraction of the Ba from the ‘preformed’ and ‘regenerated’ reservoirs respectively (with $f_{\text{pre}} + f_{\text{regen}} = 1$). This equation simulates mixing between two Ba endmembers - ‘preformed’ and ‘regenerated’ - that have fixed Ba isotope compositions. If there is no isotope fractionation accompanying regeneration processes, then the isotope composition of the regenerative flux is equivalent to those of sinking particles.

Finally the mixing of two water masses featuring different Ba concentrations and isotope compositions can be calculated as follows (eqn. 5).

$$\delta^{138/134}\text{Ba}_{\text{diss}} = [(\delta_{,1} \times [\text{Ba}]_1 \times f_1) + (\delta_{,2} \times [\text{Ba}]_2 \times f_2)] / [([\text{Ba}]_1 \times f_1) + ([\text{Ba}]_2 \times f_2)] \quad (5)$$

where δ_1 and δ_2 represent the $\delta^{138/134}\text{Ba}$ values, $[\text{Ba}]_1$ and $[\text{Ba}]_2$ the Ba concentrations, and f_1 and f_2 the fractional contributions of the two respective water masses (with $f_1 + f_2 = 1$).

The observed correlation between Ba concentrations and $\delta^{138/134}\text{Ba}$ values in the water column can be broadly reproduced by linear steady-state fractionation models, as well as non-linear regeneration and water mass mixing models (Fig. 6; Fig. 7; Fig. 8). The relatively limited range of Ba concentrations throughout the water column, of only about a factor of about 2 to 3, limits the curvature of water mass mixing lines, and hence the possibility for mixing to significantly perturb relationships between Ba concentrations and isotope compositions imparted by biogeochemical processes (Fig. 6). Likewise, because Ba is not quantitatively regenerated in the ocean interior, the observed Ba concentrations and $\delta^{138/134}\text{Ba}$ values fall on sections of the regeneration curves that can broadly approximate the observed linear relationship (Fig. 8). The similarity of trends produced by each of these types of

process, across the range of values observed in ocean waters, limits the potential for coupled Ba concentration- $\delta^{138/134}\text{Ba}$ systematics to unravel the roles of these different processes in setting the distribution of Ba in the ocean. The relatively simple Ba concentration-isotope systematics should, however, be useful for understanding the controls on the isotope compositions of particulate Ba exported to underlying sediments.

5.3 Constraining the fractionation factor associated with Ba removal from the ocean

Constraining the magnitude of the isotope fractionation accompanying Ba removal processes is crucial for understanding Ba isotope cycling in the ocean. Previous studies fit steady state fractionation models to the observed correlation between dissolved Ba concentrations and $\delta^{138/134}\text{Ba}$ values to derive fractionation factors, $\alpha_{\text{diss/part}}$ ranging from 1.00028 to 1.00058 (eqn. 3; Horner et al., 2015, Bates et al., 2017, Hsieh & Henderson, 2017). This approach is subject to uncertainty in the choice of the appropriate initial Ba concentration and $\delta^{138/134}\text{Ba}$ value (eqn. 3). This uncertainty is driven by a lack of understanding of how much of the observed variance in water column Ba concentrations and $\delta^{138/134}\text{Ba}$ values are controlled by removal versus regeneration and mixing processes. For example, Horner et al. (2015) and Bates et al. (2017) made the assumption that the distribution of dissolved Ba in the upper 1000 m to 600 m of the water column is predominantly due to variable degrees of Ba removal to particulate phases, to derive estimates of $\alpha_{\text{diss/part}}$ between 1.00028 and 1.00045. In contrast, Hsieh & Henderson (2017) assumed initial Ba concentrations and $\delta^{138/134}\text{Ba}$ of 99.7 nmol kg⁻¹ and +0.25 ‰ from waters upwelled in the Southern Ocean to derive a maximum estimated $\alpha_{\text{diss/part}}$ of 1.00058 ± 10 .

We first follow these previous approaches, but with the addition of the new data of this study to literature data (Horner et al., 2015, Bates et al., 2017, Hsieh & Henderson, 2017). Fractionation factors ($\alpha_{\text{diss/part}}$) are calculated by fitting fractionation models (eqn. 3) to linear regressions of the dissolved Ba concentrations and $\delta^{138/134}\text{Ba}$ values, with uncertainty assessed by the 95% confidence interval of the regression coefficient (Fig. 7). Taking a similar approach to Horner et al. (2015) and Bates et al. (2017), and using initial concentrations and isotope compositions of 60 nmol kg^{-1} and +0.47 ‰, yields an $\alpha_{\text{diss/part}}$ of 1.00035 ± 6 (Fig. 7a). Following a similar approach to Hsieh and Henderson (2017), using initial concentrations and isotope compositions of 100 nmol kg^{-1} and +0.25 ‰, a larger $\alpha_{\text{diss/part}}$ of 1.00052 ± 3 is obtained (Fig. 7b).

Alternative constraints on the magnitude of the isotope fractionation accompanying Ba removal from seawater can be obtained by comparing the difference in isotope composition of sinking particulate Ba to that of the waters from which this Ba is derived. The Ba isotope composition inferred for sedimentary excess Ba of $\delta^{138/134}\text{Ba} = +0.09 \pm 0.01$ ‰ (mean \pm 2SE, $n = 10$) presumably represents that of accumulated sinking particles. As validation of this assumption, isotopic mass balance models simulating the regeneration of particulate Ba (eqn. 4) can reproduce the observed relationship between dissolved Ba concentrations and isotope compositions with regenerative fluxes characterized by $\delta^{138/134}\text{Ba} = 0$ to +0.1 ‰ (Fig. 8). If there is no significant isotope fractionation accompanying Ba regeneration, which is likely in the case of BaSO_4 dissolution (von Allmen et al., 2010), these compositions provide an assessment of the globally averaged $\delta^{138/134}\text{Ba}$ values of sinking particulate Ba. These models assume the endmember scenario in which increases in dissolved Ba concentrations with depth, and associated decreases in $\delta^{138/134}\text{Ba}$ values are purely

controlled by the addition of Ba from sinking particles. This is of course an oversimplification, and there is uncertainty in the appropriate choice of ‘preformed’ Ba concentrations and $\delta^{138/134}\text{Ba}$ values. However, varying the ‘preformed’ compositions from those of South Atlantic surface waters ($\delta^{138/134}\text{Ba} = +0.6\text{‰}$; Fig. 8a), to those of deeper waters (e.g. $\delta^{138/134}\text{Ba} = +0.45\text{‰}$; Fig. 8b), makes only marginal differences in the predicted regenerative flux compositions.

The depth range over which Ba is removed from seawater to sinking particles will influence the estimated isotope fractionation because dissolved $\delta^{138/134}\text{Ba}$ values vary over the upper 1000 m of the water column (Fig. 2). The precipitation of BaSO_4 , the dominant oceanic sink of Ba, is likely to predominantly occur in the upper 500 m of the water column based on typical depths of maxima in concentrations of suspended particulate Ba (e.g. Cardinal et al., 2005, Sternberg et al., 2008, Planchon et al., 2013, Jacquet et al., 2015).

Assuming the vast majority of sinking particulate Ba, characterized by $\delta^{138/134}\text{Ba} \approx +0.1\text{‰}$, is formed in the upper 500 m of the water column, characterized by $\delta^{138/134}\text{Ba} \approx +0.5$ to $+0.6\text{‰}$, corresponds to an isotope fractionation of $\Delta^{138/134}\text{Ba}_{\text{diss-part}} = +0.4$ to $+0.5$ (or $\alpha_{\text{diss/part}} = 1.0004$ to 1.0005 ; where $\Delta^{138/134}\text{Ba}_{\text{diss-part}} = 1000 \times (\alpha_{\text{diss/part}} - 1)$). These values represent maximum estimates because sinking particulate Ba could also be removed from seawater below the specified depth, in which case it would be derived from a dissolved Ba reservoir with lower $\delta^{138/134}\text{Ba}$ values (Fig. 2). For instance, evidence from sediment trap fluxes and Ra isotopes suggesting significant components of the Ba sinking flux can be derived from several 1000 m in the water column (Dymond et al., 1992, Dymond & Collier, 1996, Dehairs et al., 2000, McManus et al., 2002, van Beek et al., 2007, 2009). The importance of Ba removal from deeper in the water column is, however, poorly known. Ultimately

the determination of suspended particulate Ba isotope compositions, particularly in the upper few hundred meters of the water column where dissolved $\delta^{138/134}\text{Ba}$ values are constant, will lead to more precise constraints. This in turn could help to better constrain the depth range over which Ba removal from the water column occurs.

5.4 Controls on the isotope composition of sedimentary excess Ba

The observed relationship between Ba concentration and isotope composition in the water column imply that the isotope fractionation associated with Ba removal must be reasonably constant throughout the ocean (Fig. 3). By assuming that the majority of excess Ba is removed from the upper 500 m of the water column, we estimate the magnitude of this isotopic fractionation to be $\Delta^{138/134}\text{Ba}_{\text{diss-part}} = +0.4$ to $+0.5$ (section 5.3). Taken together, we hypothesize that the isotope composition of excess Ba accumulating in marine sediments depends directly on the isotope composition of the dissolved Ba in upper ocean waters from which it is derived. This hypothesis can be confirmed by measurement of the isotope composition of sedimentary excess Ba across the gradients in upper ocean dissolved Ba concentrations and $\delta^{138/134}\text{Ba}$ values.

Barium isotope compositions of open ocean sediments could therefore record changes in the balance between the supply and removal of Ba from upper ocean waters, which in turn could provide constraints on export production in the past. Specifically, increased Ba supply through upwelling or external riverine inputs would act to decrease $\delta^{138/134}\text{Ba}$ values (Hsieh & Henderson, 2017), whereas increased Ba removal, related to export production, would act to increase $\delta^{138/134}\text{Ba}$ values. Upper ocean Ba concentrations are relatively homogeneous over large spatial scales due to

the importance of horizontal mixing (Hsieh & Henderson, 2017). Therefore, the dissolved Ba content of upper ocean waters, and hence Ba isotope compositions of sedimentary excess Ba, are unlikely to be significantly influenced by local biogeochemical processes, but rather record processes integrated over a broad basin scale (Hsieh & Henderson, 2017).

A particular advantage of Ba isotope composition variations for recording past perturbations to upper ocean Ba cycling, related to export production, is that they should be unaffected by uncertainty in BaSO_4 preservation rates and sediment mass accumulation rate estimates. Insights provided by Ba isotope composition variations of sedimentary excess Ba could therefore improve the application of Ba accumulation rates in sediments as a proxy for export production during periods of climatic change. For example, the recovery from the Paleocene-Eocene Thermal Maximum is marked by increases in Ba concentrations in open ocean marine sediments, which has been cited as evidence for the role of export production for the sequestration of carbon from the atmosphere-ocean system (Bains et al., 2000, Ma et al., 2014). There is however disagreement in sedimentation rates across these sedimentary sections, which imparts significant uncertainty into reconstructions of Ba accumulation rates, and thus both the timing and magnitude of changes in export production at this time period (Torfstein et al., 2010). The application of Ba isotope variations to such sediments may provide useful insights into perturbations to upper ocean Ba cycling necessary for the robust application of the Ba proxy for export production.

6. Conclusions

First constraints on the Ba isotope compositions of marine sediments are presented for samples collected along a transect extending from the Uruguayan continental margin to the mid Atlantic Ridge. The dominant control on the observed variations in Ba isotope compositions of these samples is mixing between detrital and authigenic Ba (excess Ba). These two sedimentary Ba sources exhibit rather similar isotope compositions, which will make the determination of sedimentary excess Ba isotope compositions challenging in environments that receive high inputs of detrital Ba. Open ocean sediments constrain the isotope composition of excess Ba to be $\delta^{138/134}\text{Ba} = +0.09 \pm 0.01 \text{ ‰}$ (mean \pm 2SE, $n = 10$). This is similar to that inferred for globally averaged sinking particulate Ba fluxes.

The relatively simple Ba concentration-isotope composition systematics of dissolved Ba in the water column suggests that the magnitude of the isotope fractionation accompanying removal processes is reasonable constant throughout the ocean, which is likely to be in the range +0.4 to +0.5 ‰. The isotope composition of sedimentary excess Ba is therefore hypothesized to record those of the overlying upper water column. The implications are that $\delta^{138/134}\text{Ba}$ values of sedimentary excess Ba may allow reconstruction of past perturbations in cycling of Ba in the upper ocean. In particular, changes in Ba removal rates (related to export production) and Ba supply rates (related to upwelling and possibly riverine inputs) to the upper water column should influence dissolved Ba isotope compositions, and this variation will likely be recorded by sedimentary Ba isotope signatures. Such insights should be insensitive to uncertainties in BaSO_4 preservation and sedimentation rates, and thus help better constrain the use of Ba in marine sediments as a paleo-proxy for export production.

Acknowledgements

We thank the captain, crew and science party of the *RRS James Cook* during the JC068 expedition. We also thank Phil Holdship for his role in conducting measurements of Ba and Al concentrations of sediment samples by ICP-MS, Freya Hemsing for assistance refining analytical techniques and providing Ba isotope measurements of standard reference materials, and Malcolm Woodward who performed shipboard analyses of nitrate in porewater samples. Funding for this work was in part provided by Shell Global Solutions BV. Rachel Mills (University of Southampton) supported WBH for the collection of sediments and porewater and analyses of oxygen, metals and carbon through NERC grants (NE/F017197/1 and NE/H004394/1). WBH was also supported by a NERC fellowship (NE/K009532/1). Tristan Horner, Damien Cardinal and an anonymous reviewer are thanked for their constructive comments, which helped to improve this manuscript.

References

- Anderson, R. F. & Winckler, G., 2005, Problems with paleoproductivity proxies, *Paleoceanography*, 20, 3012, doi:10.1029/2004PA001107
- Bains, S., Norris, R. D., Corfield, R. M. & Faul, K. L., 2000, Termination of global warmth at the Paleocene/Eocene boundary through productivity feedback, *Nature*, 407, 171-174
- Balakrishnan Nair, T. M., Ittekkot, V., Shankar, R. & Guptha, M. V. S., 2005, Settling barium fluxes in the Arabian Sea: Critical evaluation of relationship with export production, *Deep-Sea Research II*, 52, 1930-1946, doi:10.1016/j.dsr2.2005.06.003

596

597 Bates, S. L., Hendry, K. R., Pryer, H. V., Kinsley, C. W., Pyle, K. M., Woodward, E.
598 M. S. & Horner, T. J., 2017, Barium isotopes reveal role of ocean circulation on
599 barium cycling in the Atlantic, *Geochimica et Cosmochimica Acta*, 204, 286-299,
600 doi:10.1016/j.gca.2017.01.043

601

602 Bernstein, R. E. & Byrne, R. H., 2004, Acantharions and marine barite, *Marine*
603 *Chemistry*, 86, 45-50, doi:10.1016/j.marchem.2003.12.003

604

605 Bishop, J. K. B., 1988, The barite-opal-organic carbon association in oceanic
606 particulate matter, *Nature*, 322, 341-343

607

608 Cao, Z., Siebert, C., Hathorne, E. C., Dai, M. & Frank, M., 2016, Constraining the
609 oceanic barium cycle with stable barium isotopes, *Earth and Planetary Science*
610 *Letters*, 434, 1-9, doi:10.1016/j.epsl.2015.11.017

611

612 Cardinal, D., Savoye, N., Trull, T. W., André, L., Kopczynska, E., & Dehairs, F.,
613 2005, Variations of carbon remineralisation in the Southern Ocean illustrated by the
614 Ba_{xs} proxy, *Deep-Sea Research I*, 52, 355-370, doi:10.1016/j.dsr.2004.10.002

615

616 Dehairs, F., Chesselet, R., & Jebwab, J., 1980, Discrete suspended particles of barite
617 and the barium cycle in the open ocean, *Earth and Planetary Science Letters*, 49, 528-
618 550

619

620 Dehairs, F., Fagel, N., Antia, A. N., Peinert, R., Elskens, M. & Goeyens, L., 2000,
 621 Export production in the Bay of Biscay as estimated from barium – barite in settling
 622 material: a comparison with new production, *Deep-Sea Research I*, 47, 583-601
 623
 624 Dickens, G., Fewless, E., Thomas, E. & Bralower, T., 2003, Excess barite
 625 accumulation during the Paleocene/Eocene thermal maximum: Massive input of
 626 dissolved barium from seafloor gas hydrate reservoirs, *in* Ginerich, P., et al., eds.,
 627 Causes and consequences of globally warm climates in the early Paleogene:
 628 Geological Society of America Special Paper 369, p. 11-23
 629
 630 Dymond, J., Suess, E. & Lyle, E., 1992, Barium in deep-sea sediment: A geochemical
 631 proxy for paleoproductivity, *Paleoceanography*, 7 (2), 163-181
 632
 633 Dymond, J. & Collier, R., 1996, Particulate barium fluxes and their relationships to
 634 biological productivity, *Deep-Sea Research II*, 43, 1283-1308
 635
 636 Eagle, M., Paytan, A., Arrigo, K. R., van Dijken, G. & Murray, R. W., 2003, A
 637 comparison between excess barium and barite as indicators of carbon export,
 638 *Paleoceanography*, 18, 1, 1021, doi:10.1029/2002PA000793
 639
 640 Fagel, N., Dehairs, F., Andre, L., Bareille, G. & Monnin, C, 2002, Ba distribution in
 641 surface Southern Ocean sediments and export production estimates,
 642 *Paleoceanography*, 17 (2), 1011, doi:10.1029/2000PA000552
 643

644 Foster, D. A., Staubwasser, M. & Henderson, G. M., 2004, ^{226}Ra and Ba
 645 concentrations in the Ross Sea measured with multicollector ICP mass spectrometry,
 646 *Marine Chemistry*, 87, 59-71, doi:10.1016/j.marchem.2004.02.003
 647
 648 Francois, R., Honjo, S., Manganini, S. J. & Ravizza, G. E., 1995, Biogenic barium
 649 fluxes to the deep sea: Implications for paleoproductivity reconstruction, *Global*
 650 *Biogeochemical Cycles*, 9 (2) 289-303
 651
 652 Ganeshram R. S., François, R., Commeau, J. & Brown-Leger, S. L., 2003, An
 653 experimental investigation of barite formation in seawater, *Geochimica et*
 654 *Cosmochimica Acta*, 67 (14), 2599-2605
 655
 656 Gingele, F. & Dahmke, A., 1994, Discrete barite particles and barium as tracers of
 657 paleoproductivity in South Atlantic sediments, *Paleoceanography*, 9 (1), 151-168
 658
 659 Homoky, W.B., Hembury, D.J., Hepburn, L.E., Mills, R.A., Statham P.J., Fones, G. &
 660 Palmer, M. 2011 Iron and Manganese diagenesis in deep sea volcanogenic sediments
 661 and the origins of pore water colloids. . *Geochim. Cosmochim. Acta* **75**, 5032-5048.
 662
 663 Homoky, W. B., John, S. G., Conway, T. M. & Mills, R. A., 2013, Distinct iron
 664 isotopic signatures and supply from marine sediment dissolution, *Nature*
 665 *Communications*, 4, 2143, doi:10.1038/ncomms3143
 666
 667 Hoppema, M., Dehairs, F., Navez, J., Monnin, C., Jeandel, C., Fahrbach, E. & de
 668 Baar, H. J. W., 2010, Distribution of barium in the Weddell Gyre: Impact of

669 circulation and biogeochemical processes, *Marine Chemistry*, 122, 118-129,
670 doi:10.1016/j.marchem.2010.07.005
671
672 Horner, T. J., Kinsley, C. W. & Nielsen, S. G, 2015, Barium isotope fractionation in
673 seawater mediated by barite cycling and oceanic circulation, *Earth and Planetary*
674 *Science Letters*, 430, 511-522, doi:10.1016/j.epsl.2015.07.027
675
676 Hsieh, Y-T. & Henderson, G. M., 2017, Barium stable isotopes in the global ocean:
677 Tracer of Ba utilization and inputs, *Earth and Planetary Science Letters*, 473, 269-
678 278, doi.org/10.1016/j.epsl.2017.06.024
679
680 Jacquet, S. H. M., Dehairs, F., Lefevre, D., Cavagna, A. J., Planchon, F., Christaki,
681 U., Monin, L., André, L., Closset, I. & Cardinal, D, 2015, Early spring mesopelagic
682 carbon remineralization and transfer efficiency in the naturally iron-fertilized
683 Kerguelen area, *Biogeosciences*, 12, 1713-1731, doi:10.5194/bg-12-1713-2015
684
685 Jacquet, S. H. M., Monnin, C., Riou, V., Jullion, L. & Tanhua, T., 2016, A high
686 resolution and quasi-zonal transect of dissolved Ba in the Mediterranean Sea, *Marine*
687 *Chemistry*, 178, 1-7, doi:10.1016/j.marchem.2015.12.001
688
689 Jeandel, C., Dupré, B., Lebaron, G., Monnin, C. & Minster, J. F., 1996, Longitudinal
690 distributions of dissolved barium, silica and alkalinity in the western and southern
691 Indian Ocean, *Deep-Sea Research I*, 43 (1), 1-31
692

693 Klump, J., Hebbeln, D. & Wefer, G., 2000, The impact of sediment provenance on
694 barium-based productivity estimates, *Marine Geology*, 169, 259-271
695

696 Legeleux, F. & Reyss, J-L, 1996, $^{228}\text{Ra}/^{226}\text{Ra}$ activity ratio in oceanic settling
697 particles: implications regarding the use of barium as a proxy for paleoproductivity
698 reconstruction, *Deep-Sea Research I*, 45 (11-12), 1857-1863
699

700 Mawji et al., 2015, The GEOTRACES intermediate data product 2014, *Marine*
701 *Chemistry*, 177 (1), 1-8, doi:10.1016/j.marchem.2015.04.005
702

703 Ma, Z., Gray, E., Thomas, E., Murphy, B., Zachos, J. & Paytan, A., 2014, Carbon
704 sequestration during the Palaeocene-Eocene Thermal Maximum by an efficient
705 biological pump, *Nature Geoscience*, 7, 382-388, doi:10.1038/NGEO2139
706

707 McManus, J., Dymond, J., Dunbar, R. B. & Collier, R. W, 2002, Particulate barium
708 fluxes in the Ross Sea, *Marine Geology*, 184, 1-15
709

710 Monnin, C., Jeandel, C., Cattaldo, T, & Dehairs, F., 1999, The marine barite
711 saturation state of the world's oceans, *Marine Chemistry*, 65, 253-261
712

713 Nan, X., Wu, F., Zhang, Z., Hou, Z., Huang, F, & Yu, H., 2015, High-precision
714 barium isotope measurements by MC-ICP-MS, *Journal of Analytical Atomic*
715 *Spectrometry*, doi:10.1039/c5ja00166h
716

717 Paytan, A., & Griffiths, E. M., 2007, Marine barite: Recorder of variations in ocean
 718 export productivity, *Deep-Sea Research II*, 54, 687-705,
 719 doi:10.1016/j.dsr2.2007.01.007
 720
 721 Paytan, A & Kastner, M., 1996, Benthic Ba fluxes in the central Equatorial Pacific,
 722 implications for the oceanic Ba cycle, *Earth and Planetary Science Letters*, 142, 439-
 723 450
 724
 725 Pfeifer, K., Kasten, S., Hensen, C. & Schulz, H. D., 2001, Reconstruction of primary
 726 productivity from the barium contents in surface sediments of the South Atlantic
 727 Ocean, *Marine Geology*, 177, 13-14
 728
 729 Planchon, F., Cavagna, A.-J., Cardinal, D., André, L. & Dehairs, F., 2013, Late
 730 summer particulate organic carbon export and twilight zone remineralisation in the
 731 Atlantic sector of the Southern Ocean, *Biogeosciences*, 10, 8030820, doi:10.5194/bg-
 732 10-803-2013
 733
 734 Reitz, A., Pfeifer, K., de Lange, G. J. & Klump, J., 2004, Biogenic barium and the
 735 detrital Ba/Al ratio: a comparison of their direct and indirect determination, *Marine*
 736 *Geology*, 204, 289-300, doi:10.1016/S0025-3227(04)00004-0
 737
 738 Schlitzer, R., (2015), Ocean Data View, <http://odv.awi.de>
 739
 740 Sternberg, E., Jeandel, C, Miquel, J. C., Gasser, B, Souhaut, M, Arraes-Mescoff, R. &
 741 Francois, R., 2007, Particulate barium fluxes and export production in the

742 northwestern Mediterranean, *Marine Chemistry*, 105, 281-295,
 743 doi:10.1016/j.marchem.2007.03.003
 744
 745 Sternberg, E., Jeandel, C, Robin, E., & Souhaut, M., 2008, Seasonal cycle of
 746 suspended barite in the mediterranean sea, , *Geochimica et Cosmochimica Acta*, 72,
 747 4020-4034, doi:10.1016/j.gca.2008.05.043
 748
 749 Sternberg, E., Tang, D., Ho, T-Y., Jeandel, C. & Morel, F. M. M., 2005, Barium
 750 uptake and adsorption in diatoms, *Geochimica et Cosmochimica Acta*, 69, 2745-2752
 751
 752 Torres, M. E., Brumsack, H. J., Bohrmann, G. & Emeis, K. C., 1996, Barite fronts in
 753 continental margin sediments: A new look at barium remobilization in the zone of
 754 sulfate reduction and formation of heavy barites in diagenetic fronts, *Chemical*
 755 *Geology*, 127, 125-139
 756
 757 Torfstein, A., Winckler, G. & Tripathi, A., 2010, Productivity feedback did not
 758 terminate the Paleocene-Eocene Thermal Maximum (PETM), *Climate of the Past*, 6,
 759 265-272
 760
 761 van Beek, P., François, R., Conte, M., Reyss, J-L., Souhaut, M. & Charette, M., 2007,
 762 $^{228}\text{Ra}/^{226}\text{Ra}$ and $^{226}\text{Ra}/\text{Ba}$ ratios to track barite formation and transport in the water
 763 column, *Geochimica et Cosmochimica Acta*, 71, 71-86,
 764 doi:10.1016/j.gca.2006.07.041
 765

van Beek, P., Sternberg, E., Reyss, J-L., Souhaut, M., Robin, E. & Jeandel, C., 2009,
 $^{228}\text{Ra}/^{226}\text{Ra}$ and $^{226}\text{Ra}/\text{Ba}$ ratios in the Western Mediterranean Sea: Barite formation
and transport, *Geochimica et Cosmochimica Acta*, 73, 4720-4737,
doi:10.1016/j.gca.2009.05.063

von Allmen, K., Böttcher, M. E., Samankassou, E., Nägler, T. F., 2010, Barium
isotope fractionation in the global barium cycle: First evidence from barium minerals
and precipitation experiments, *Chemical Geology*, 277, 70-77,
doi:10.1016/j.chemgeo.2010.07.011

Wyatt, N. J., Milne, A., Woodward, E. M. S., Rees, A. P., Browning, T. J., Bouman,
H. A., Worsfold, P. J. & Lohan, M. C., 2014, Biogeochemical cycling of dissolved
zinc along the GEOTRACES South Atlantic transect GA10 at 40°S, *Global
Biogeochemical Cycles*, 28, 44-56, doi:10.1002/2013GB004637

Figure 1; Sampling locations for seawater depth profiles and sediment cores. Panel
(a) shows map of station (stn) locations for collection of seawater depth profiles
(circles) and sediment cores (squares). Note that the results for the seawater depth
profile at station 20 have been previously published (Hsieh & Henderson, 2017).
Panel (b) displays a vertical section of salinity along the GEOTRACES GA10 section,
with sampling locations. The main water masses are labeled; AAIW – Antarctic
Intermediate Water, UCDW – Upper Circumpolar Deep Water, NADW – North
Atlantic Deep Water, AABW – Antarctic Bottom Water. Also shown is the location
of seawater depth profiles for Ba concentrations and isotope compositions published

by Horner et al. (2015), at station 6, and Bates et al. (2017), at station 3. Figure produced using Ocean Data View (Schlitzer, 2015).

Figure 2; Seawater depth profiles of dissolved Ba concentrations (open circles) and $\delta^{138/134}\text{Ba}$ values (closed circles). Panels (a) to (e) display results for the upper 1000 m of the water column on an expanded scale, while panels (f) to (i) display results for the full range of depths. Note that results for station 22 only extend down to 996 m. Results for station 20 have been previously presented by Hsieh & Henderson (2017).

Figure 3; Relationship between dissolved Ba concentrations and $\delta^{138/134}\text{Ba}$ values for seawater samples. Displayed are results from the South Atlantic (this study, Horner et al., 2015, Bates et al., 2017, Hsieh & Henderson, 2017), as well as literature values for the North Atlantic, Southern Ocean and North Pacific (Bates et al., 2017, Hsieh & Henderson, 2017), which display a consistent relationship. Note that results published by Cao et al. (2016) have been excluded from the compilation as they exhibit a different relationship between these parameters, with higher $\delta^{138/134}\text{Ba}$ values.

Figure 4; Elemental and Ba isotope composition results for the sediment cores as a function of depth below seafloor. The proportions of non-detrital Ba ($\text{Ba}_{\text{excess}}$) are estimated assuming a detrital Ba/Al ratio of 0.0055 ± 0.0005 .

Figure 5; The relationship between estimated proportions non-detrital Ba ($\text{Ba}_{\text{excess}}$) versus $\delta^{138/134}\text{Ba}$ values for the sediment samples. The fractional contributions of excess Ba are calculated assuming a detrital Ba/Al ratio of 0.0055 ± 0.0005 .

Figure 6; Bimodal mixing trends between waters with different Ba concentrations and $\delta^{138/134}\text{Ba}$ values, spanning the observed range of values in the water column. The light grey, dark grey and black lines show mixing between South Atlantic surface waters (40 nmol kg⁻¹, and $\delta^{138/134}\text{Ba} = +0.6 \text{ ‰}$), and waters with 50 nmol kg⁻¹/ $\delta^{138/134}\text{Ba} = +0.5 \text{ ‰}$, 70 nmol kg⁻¹/ $\delta^{138/134}\text{Ba} = +0.37 \text{ ‰}$ and 100 nmol kg⁻¹/ $\delta^{138/134}\text{Ba} = +0.25 \text{ ‰}$ respectively. The chosen endmembers are not intended to reproduce any specific mixing scenarios expected to be important, only to demonstrate a range of theoretically possible mixing relationships. Note that the degree of curvature of the mixing trends decreases with decreasing difference in Ba concentrations of the two water masses (eqn. 5). Literature dissolved Ba concentration and isotope composition data are from Horner et al. (2015), Bates et al., (2017) and Hsieh & Henderson (2017).

Figure 7; Isotope fractionation models explaining the observed relationship between dissolved Ba concentrations and isotope compositions in the water column. Panels (a) and (b) display steady state fractionation models assuming Ba removal from waters with an initial Ba concentrations of 60 nmol kg⁻¹ and 100 nmol kg⁻¹ respectively (i.e. following the approaches of Bates et al. (2017) and Hsieh and Henderson (2017) respectively; see section 5.3). Fractionation factors ($\alpha_{\text{diss/part}}$) are derived by fitting fractionation models (eqn. 3) to linear regressions of the data, with uncertainty assessed using the 95% confidence interval of the regression coefficient (dashed lines). The predicted isotope compositions of resulting particulate phases are constrained by the fractionation factor. The isotope composition of sedimentary excess Ba, defined by sediments of station 8 (e.g. Fig 5) is shown as a brown line for reference. The grey shaded areas highlight the isotope composition of particulate Ba

predicted to form from waters in the upper 500 m featuring $\delta^{138/134}\text{Ba} = +0.5$ to $+0.6$ ‰. Approximate water depths corresponding to the dissolved Ba concentrations and $\delta^{138/134}\text{Ba}$ values for Atlantic data are labeled. Literature dissolved Ba concentration and isotope composition data are from Horner et al. (2015), Bates et al., (2017) and Hsieh & Henderson (2017).

Figure 8; Isotope mass balance models explaining the observed variance in dissolved Ba concentrations and isotope compositions in terms of the addition of Ba through the regeneration of sinking particulate Ba. Panels (a) and (b) display regeneration models assuming a pre-formed Ba concentration and $\delta^{138/134}\text{Ba}$ value of 40 nmol kg⁻¹ and $+0.6$ ‰ and 60 nmol kg⁻¹ and $+0.45$ ‰ respectively (eqn. 4), and are intended to illustrate the effect of varying the pre-formed endmember on the model calculations. For each model, the isotope composition of the regenerated particulate Ba is labeled. Literature dissolved Ba concentration and isotope composition data are from Horner et al. (2015), Bates et al., (2017) and Hsieh & Henderson (2017).

Figure 1

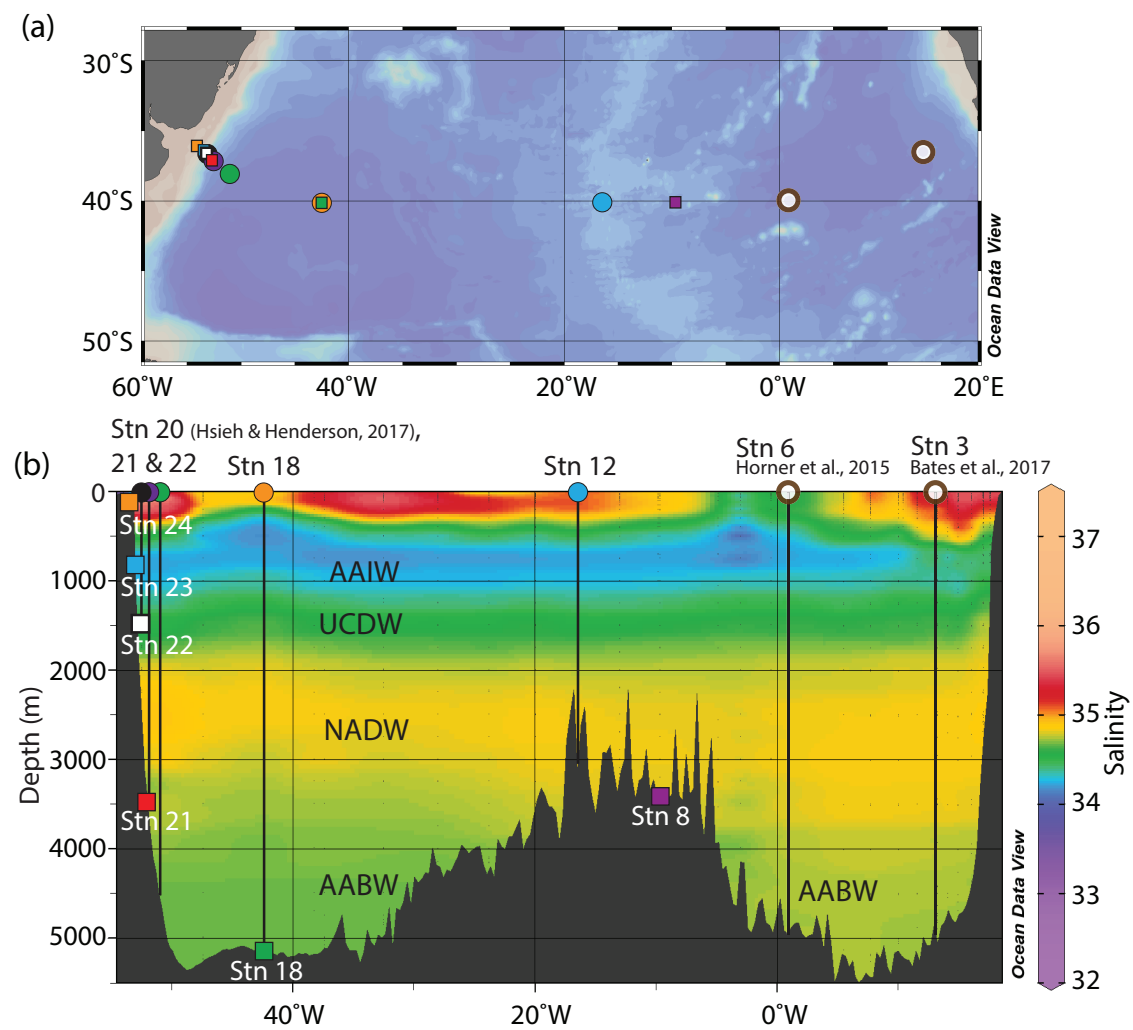


Figure 2

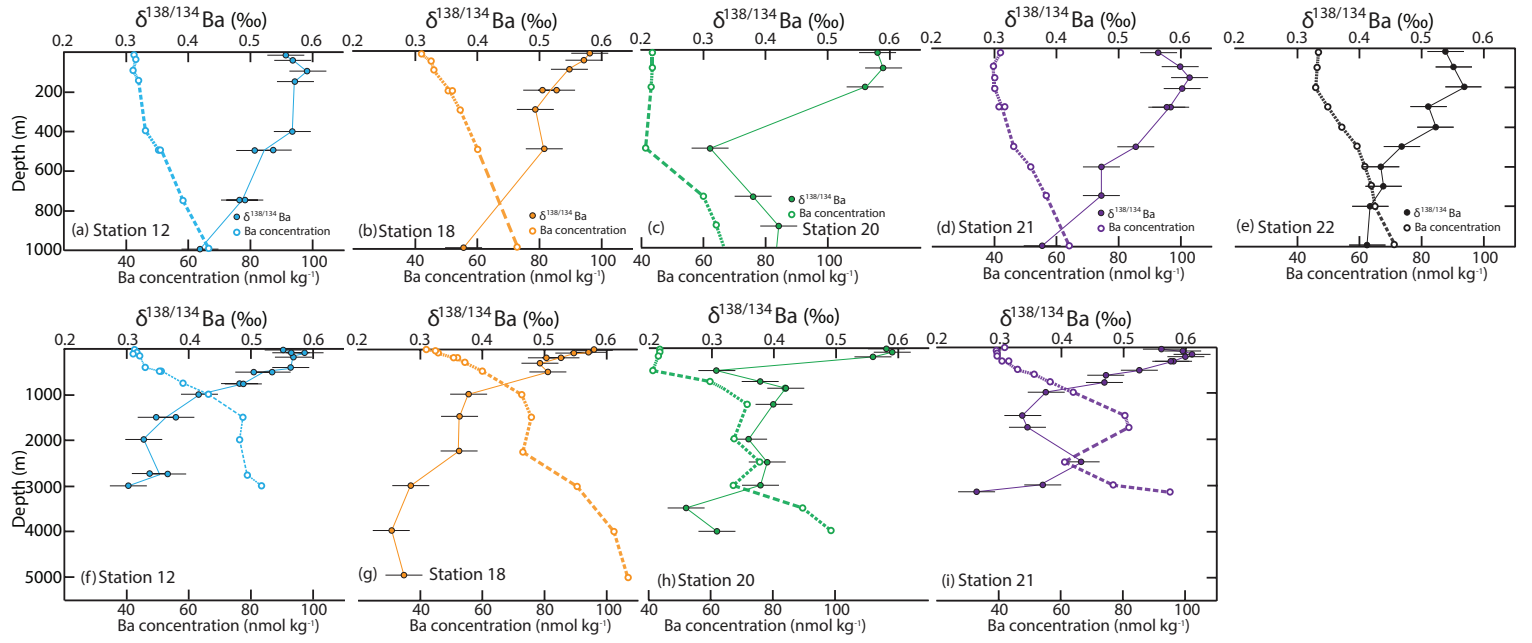


Figure 3

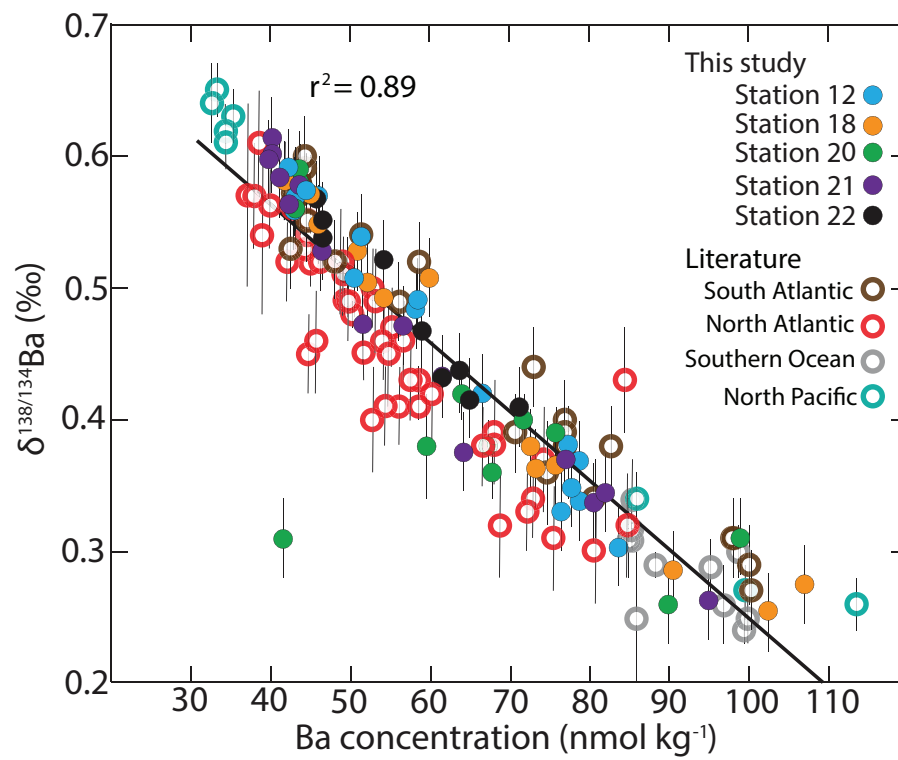


Figure 4

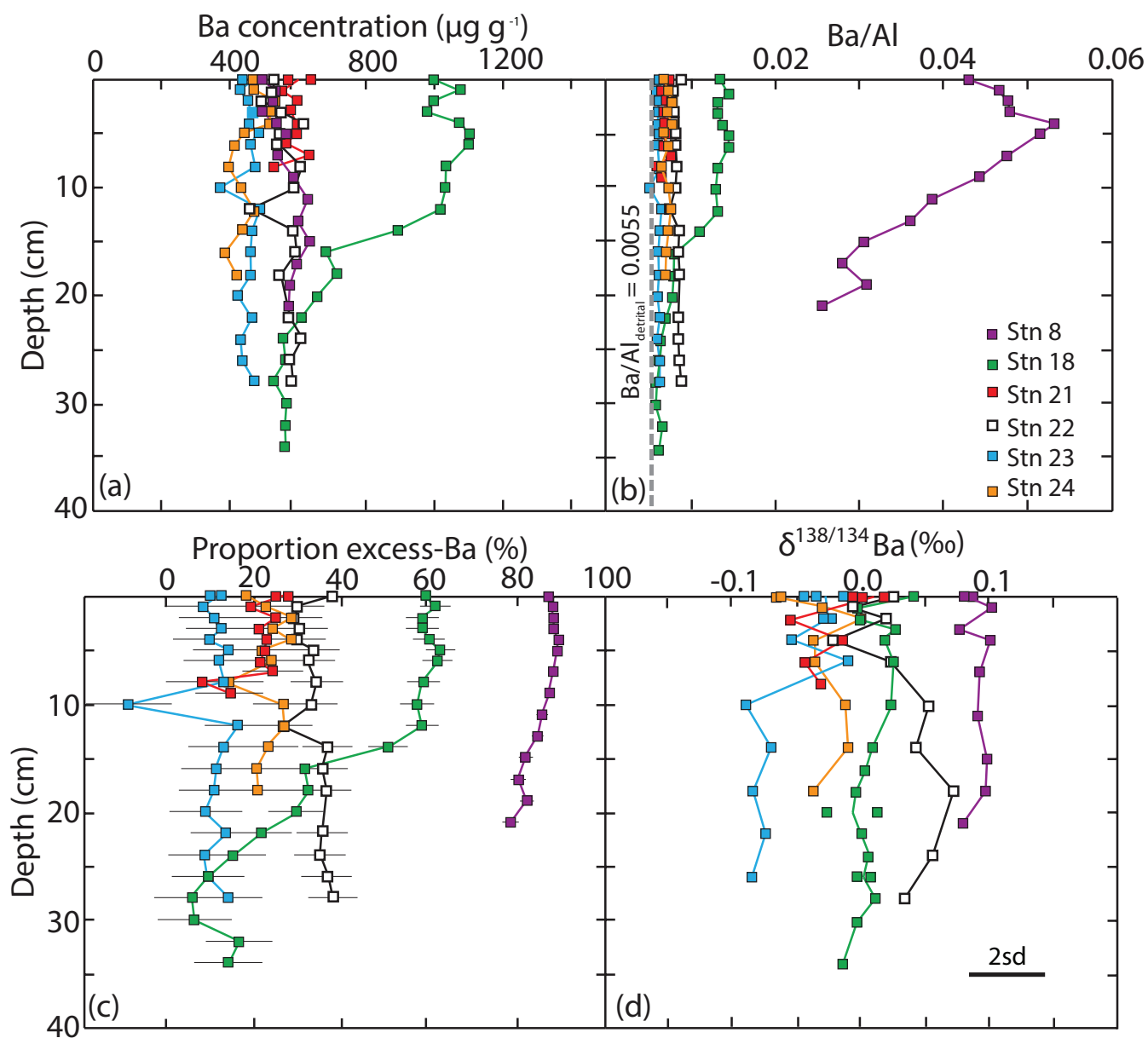


Figure 5

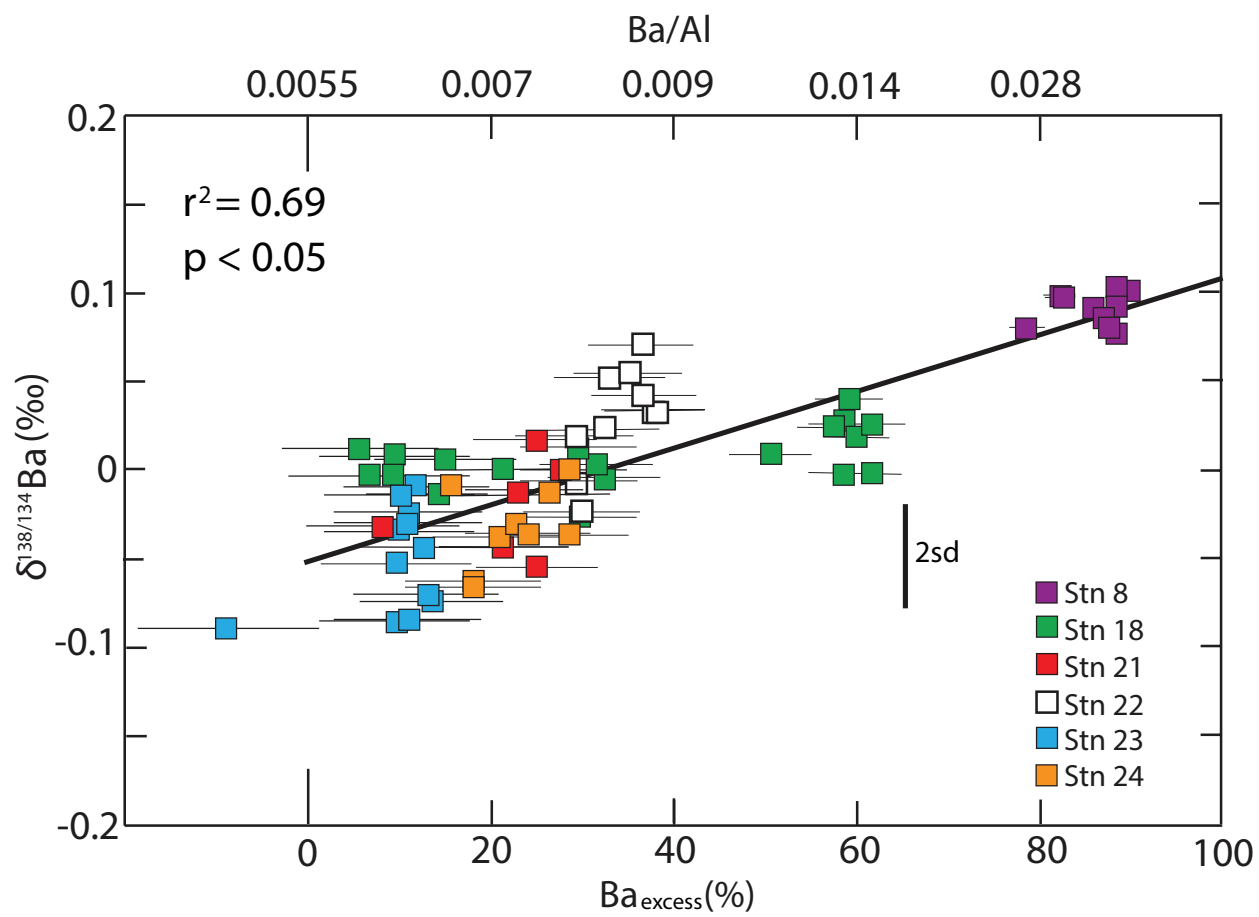


Figure 6

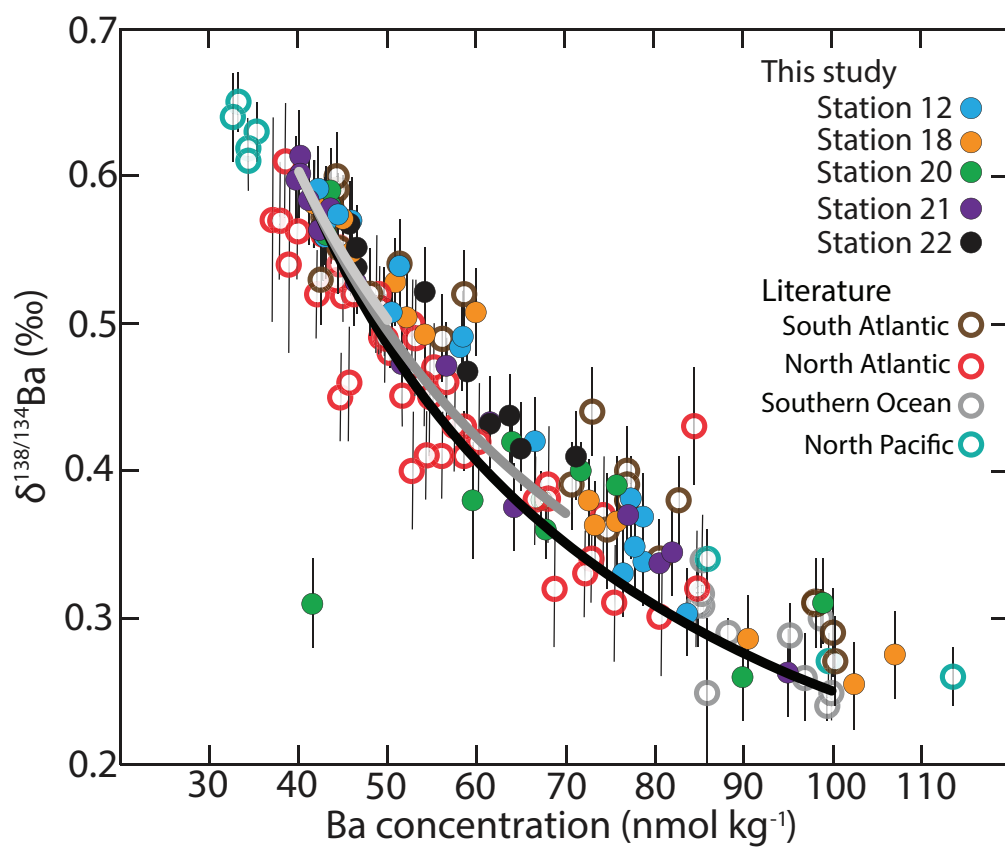


Figure 7

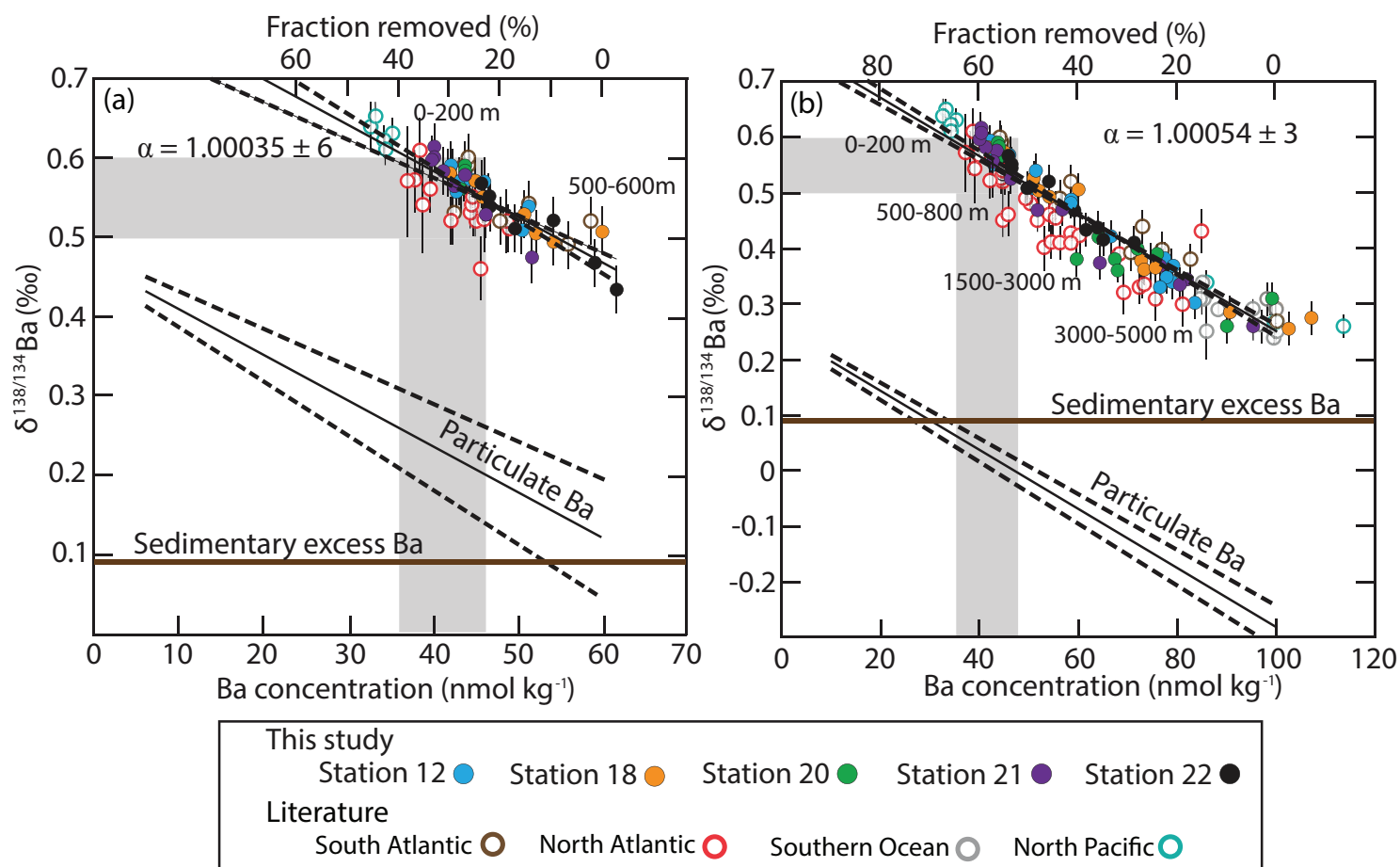


Figure 8

